Common mode modelling and filter design for a three-phase buck-type pulse width modulated rectifier system

M.L. Heldwein[1]   *T. Nussbaumer*[2]   *J.W. Kolar*[3]

[1]*Electrical Engineering Department, Federal University of Santa Catarina, 88040-970 Florianópolis, Brazil*
[2]*Levitronix GmbH, 8005 Zurich, Switzerland*
[3]*Power Electronic Systems Laboratory, Swiss Federal Institute of Technology (ETH), 8092 Zurich, Switzerland*
*E-mail: heldwein@inep.ufsc.br*

Abstract: The EMC input filter design for a three-phase pulse width modulated (PWM) rectifier is usually separated into the design of the differential mode (DM) and common mode (CM) stages. While for the DM filter design rules and procedures are well known and easier to predict, the CM filter design is often based on trial-and-error methods and/or on the experience of the designer. In the present study, a comprehensive design procedure for a CM EMC input filter is performed for a three-phase three-switch buck-type PWM rectifier. A model of the CM noise propagation is developed and the relevant parasitic impedances are identified. A capacitive connection from the star-point of the DM input filter to the capacitive centre point of the rectifier output voltage is proposed and the effect of this measure-concerning CM is verified. Finally, a two-stage CM filter is designed and compliance to the conducted emission (CE) requirements of CISPR 22 Class B is verified through measurements on a 5 kW prototype.

1 Introduction

Three-phase pulse width modulated (PWM) rectifiers are frequently employed in utility interfaced systems. They are technically attractive for presenting smaller dimensions, lower cost, high efficiency and improved electrical performance when compared to other solutions [1]. On the other hand, PWM converters are, in general, less robust and generate high-frequency harmonic contents. The three-phase buck-type PWM rectifier (cf. Fig. 1) has been presented in the literature [2] and is well suited for utility interfaced systems, where the rectified output voltage is required to be lower than the input voltages and the input currents are required to be of high quality [3–5]. The integration of a boost-type output stage as in [6–8] allows for higher output voltages employing the same input stage. This type of system finds its application in telecommunication energy systems or as front-end for various applications such as plasma power supplies, process technology and others.

Owing to the discontinuous input currents of this system [2], at least a single-stage LC differential mode (DM) input filter is required, however, for full compliance to EMC standards [9, 10] the conducted DM and common mode (CM) conducted emissions (CE) propagating to the mains have to be sufficiently attenuated. For this reason, EMC input filters must be employed with this rectifier. Since the DM filter mainly defines the power density, the low-load power factor and the dynamics of the system, it is advantageous to design this filter stage in a first step, by employing either a numerical calculation procedure or using a CM/DM separator as presented in [11]. For the rectifier employed here, the DM filter stage designed in [5] is used and a photograph of the built prototype is depicted in Fig. 2. Furthermore, the DM filter components influence the behaviour of common mode current propagation and are, therefore required for a proper CM modelling procedure.

The circulation of high-frequency currents between the power lines and the protective earth conductors, named
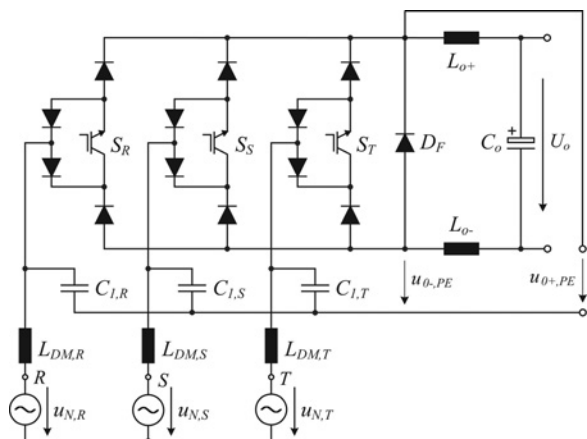
Figure 1 *Structure of the power circuit of a three-phase three-switch buck PWM rectifier designed for the realisation of the input stage of a 5 kW telecommunications power supply module switching at $f_p = 28$ kHz*

For clarity, only the DM filter components, which are relevant for the CM filter design ($L_{DM,i}$ and $C_{1,i}$) are shown, where $L_{DM,i}$ is the sum of all DM filter inductances of a phase

CM currents, lead to potential electromagnetic interference (EMI), since this noise mode is typically responsible for the larger portion of radiated emissions. Input CM filters act on reducing these currents, thus, decreasing the possibility of EMI. These filters are employed for two main reasons: (i) preventing emissions from the considered converter to interfere with neighbouring equipments, and (ii) on the other way around, avoiding the disturbance of the converter by sources of electromagnetic noise in the surrounding environment [9, 10]. Nevertheless, these filters have their design driven mainly by international EMC standards, which put limits to the amount of emissions that an equipment can emit. Another similarity to DM filters is that these filters typically occupy a significant amount of space in a power converter.
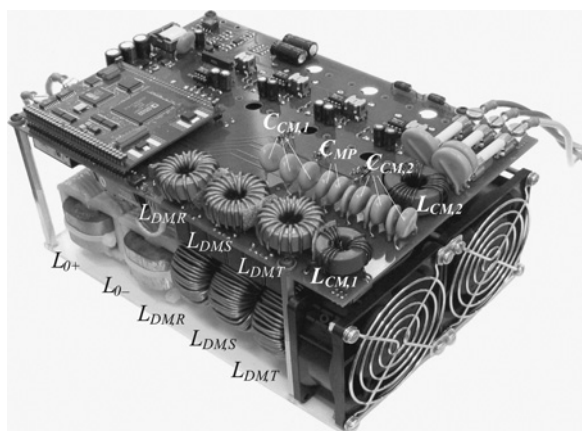
Figure 2 *Three-phase buck-type PWM rectifier 5 kW hardware prototype including the CM filter, the DM filter, auxiliary power supply and the DSP control board (160 × 240 × 120 mm)*

Differently from DM filters, the CM filters employ relatively high inductances and low capacitance values. High inductances can be used because of the characteristics of CM chokes, which employ high permeability materials, thus achieving high impedances with limited amount of magnetic material. The small capacitances employed in a CM filter come from restrictions because of safety regulations, which limit the amount of current that can flow in such capacitors. Even though the objectives are similar, the design of CM filters is a quite distinct task when compared to the design of DM ones.

The CM filter design is often based on trial-and-error methods and/or on the experience of the designer because of the inherently difficult prediction of the CM noise source characteristics in a complex power electronics systems [9, 12–14]. Models for CM prediction have been proposed for boost-type rectifiers [15–17], where efforts are put on the numerical or mathematical modelling of the noise paths and sources. However, if a prototype of the system is available, which can be used for the EMC evaluation, models based on hardware measurements can be derived.

The proper identification of the noise spectra allows, along with the determination of relevant noise paths, for the early determination of filtering requirements and possibilities and, thus, for an efficient filter design. For the specific case of three-phase converters the exact analytic calculation of such spectral contents is of high complexity [18, 19] and sometimes varying upon operating conditions. Therefore simplifications are typically performed. Other methods include numerical simulation with varying degree of complexity and direct hardware measurements.

Computer-based simulations and analytical models vary in modelling complexity according to the applied efforts. Simulations aiming for EMC purposes might model a multiphysics environment involving three-dimensional electromagnetic field solvers, heat flow dynamics, control strategies, calculations of losses and electric circuits solvers. These simulations are not yet common, since the computational effort is immense. Most of today's modelling procedures neglect to some extent the couplings among different physical domains. The advantages of numerical simulations are the easiness of modifying important parameters, reduced costs and study of the effects of each part of the circuit. The precision of a simulation relies not only on the software, but most importantly in the construction of the model.

The EMC modelling of power converters based on direct hardware measurements [20–22, 12] has, over other methods, the advantage of including all electromagnetic and thermal effects involved in the system. The obvious disadvantages of this type of modelling are the difficulties of implementing modifications and the uncertainties of not knowing exactly which mechanisms generate the observed effects. In a last step before EMC certification this method is, of course, employed and the engineering skills of the

designers are required to assess the compliance of the equipment or to realise required improvements when necessary.

The three approaches, analytic calculation, simulation and experiments, can be coupled together in different design stages. The proper management and coordination of these tasks, allied to tacit experience, leads to appropriate models and subsequent EMC compliance. In this work, a procedure based on the combination of simulation and experimental results is proposed in order to model the converter from a CM perspective. Furthermore, applying the achieved model allows for the design of CM filters. Such approach can be extended to other topologies, so that CM emissions can be successfully controlled.

This paper is structured as follows. In Section 2, a CM noise propagation model is derived, which is based on the relevant parasitic impedances, identified through measurements and on the simulation analysis of the generation of CM voltages in the power topology. Section 3 presents the performed CM filter design. The effect of an HF connection of the star-point of the DM input filter capacitors to the output of the rectifier is proposed and analysed concerning its effect on the modelled CM noise paths. A two-stage conventional CM input filter is designed and the selection of filter components aiming to achieve the required attenuation is presented. Furthermore, the attenuation of the employed filtering elements is analysed. Finally, the compliance to CISPR 22 Class B limits is verified through CE measurements on a 5 kW prototype employing the designed CM filter.

2 CM model of a three-phase buck-type PWM rectifier system

In order to successfully design a CM filter, an equivalent CM noise source model is required [12]. The objective of this section is to derive a simplified equivalent CM noise propagation model, where the relevant parasitic impedances are identified through impedance measurements. This model shall be valid for the frequency range, where the main CM filter components are to be designed.

As the CM currents circulate through parasitic distributed capacitances, which are very complex to model as distributed parameters, simplified lumped elements are used to model the main current paths. This assumption reduces the frequency range of the model.

The main propagation paths of the CM current are modelled as shown in Fig. 3. The CM current paths are closed through the parasitic capacitances ($C_{\text{MP–GND}}$, $C_{\text{Co–GND}}$ and $C_{\text{Ro–GND}}$) between the PE terminal, the heatsink and the elements of the power circuit. For the CM current the three phases are lying in parallel, therefore one-third of the DM input filter inductors value becomes effective as depicted in Fig. 4, and one-third of the test receiver sensing input resistance $R_{\text{LISN},i}$ is seen by the CM current. The CM current i_{CM} through the DM inductors $L_{\text{DM},i}$ into the mains causes an according noise level at the grid or LISN network in case of CE testings. Assuming, because of $L_{\text{LISN},i}$, at high frequencies, an ideal decoupling of the EUT to the mains, and a perfect coupling with the test receiver, through $C_{\text{LISN},i}$ in a simplified consideration, the equivalent high-frequency circuit Fig. 4 is obtained and only low-frequency components circulate to the mains ($i_{\text{CM,LF}}$). The capacitance $C_{\text{MP–GND}}$ is the lumped capacitance model for the high-frequency connection between the power modules (S_R, S_S, S_T) and the heatsink. It is drawn in Fig. 3 connected to the negative rail since a higher capacitance is observed at the anodes of the diodes.

On the DC side of the rectifier circuit, the two DC inductances $L_{\text{o+}} = L_{\text{o−}} = L_{\text{o}}/2$ are in parallel for CM. If the distributed capacitances from the output capacitors to PE are summed into a single total capacitance $C_{\text{Co–GND}}$, one path with the output capacitance $4C_{\text{o}}$ results. The capacitance $C_{\text{Co–GND}}$ models the influence of the parasitic capacitive connection from the printed circuit board output traces to the heatsink. This capacitance is placed in the centre point of the output capacitors because of the large plane in the PCB placed with this potential. The distributed capacitances from the load resistor to ground are modelled through $C_{\text{Ro–GND}}$ from the load middle-point to ground, which results in a path with $R_{\text{o}}/4$.
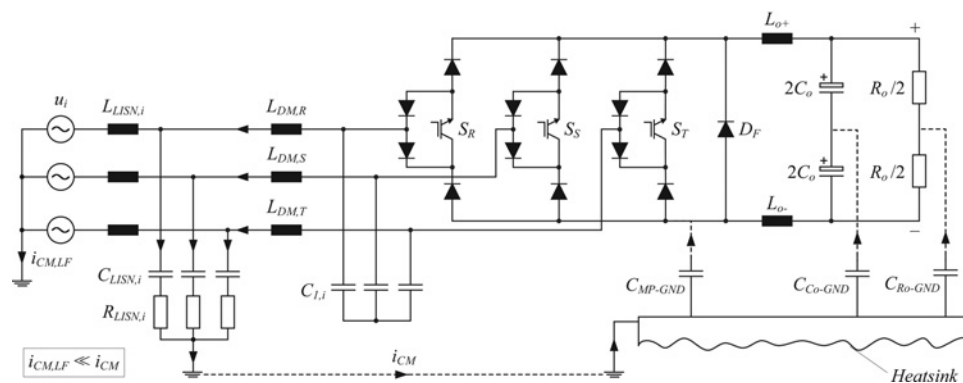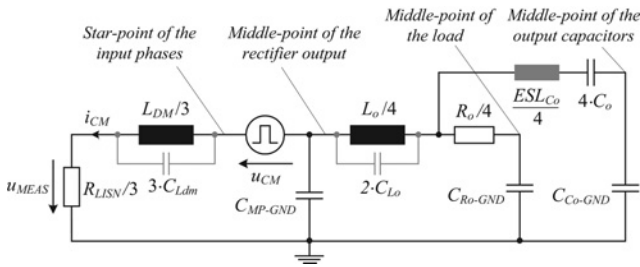

Figure 3 *Propagation model of the common mode currents in the rectifier system used for deriving the CM noise model*

**Figure 4** *CM noise propagation model for the three-phase buck-type PWM rectifier*

Components values: $L_{DM} = 270\,\mu H$; $L_o = 2\,mH$; $C_o = 750\,\mu F$; $C_{MP-GND} = 141\,pF$; $C_{Ro-GND} = 57\,pF$; $C_{Co-GND} = 283\,pF$

The main parasitic components of the DM filter inductors and output inductors are modelled with the parasitic capacitances C_{Ldm} and C_{Lo}. The equivalent series inductance of the output foil capacitors is modeled with ESL_{Co}.

The rectifier itself is modelled as a common mode voltage source u_{CM} that drives the potential between the star-point of the rectifier input (lying at the star-point of the DM input filter capacitors, which are not relevant for the CM noise model) and the middle-point of the rectifier output.

2.1 Estimation of the model parameters

For the measurement and estimation of the relevant capacitances (C_{MP-GND}, C_{Co-GND} and C_{Ro-GND}), a series of impedance measurements are performed with a precision impedance analyser Agilent 4294A. For evaluating C_{Ro-GND} an impedance measurement is done with disconnected power cables, leading to a high-frequency equivalent circuit presenting a resistor, an inductor and a capacitor in series, from which only the capacitance value is used in this design procedure and has a value of $C_{Ro-GND} = 57\,pF$. The same procedure is applied to measure the impedance of the output capacitors and of the output inductors. The results for these components are displayed in Fig. 6. The DM filter inductors $L_{DM,i}$ are
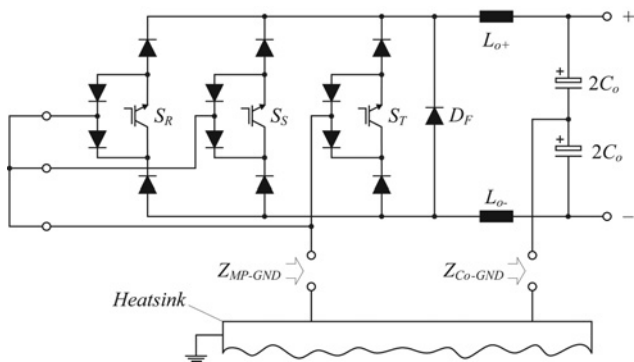
Figure 5 *Setup for the impedance measurements performed in order to evaluate the CM noise paths within the rectifier prototype*
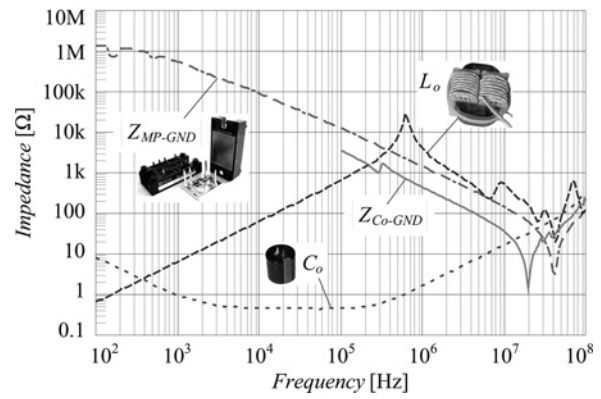
Figure 6 *Measured impedances: output inductors L_o, output capacitors C_o, impedance Z_{MP-GND} and Z_{Co-GND} as defined in Fig. 5*

modelled as a parallel connection of $R = 3\,k\Omega$, $L = 270\,\mu H$ and $C = 52\,pF$.

Since the capacitances C_{MP-GND} and C_{Co-GND} are dependent on the complete converter layout, they are indirectly estimated with two impedance measurements. The rectifier is disconnected from the mains and the load and the impedances Z_{Co-GND} and Z_{MP-GND} are measured according to the setup shown in Fig. 5. The results from these measurements are presented in Fig. 6.

By considering the two equivalent circuits (cf. Fig. 5) resulting from each impedance measurement, two simplified equations for the two unknown parameters C_{MP-GND} and C_{Co-GND} can be derived resulting in

$$Z_{MP-GND} \cong \frac{1/s\,C_{MP-GND} \cdot (s(L_o/4) + 1/s\,C_{Co-GND})}{1/s\,C_{MP-GND} + (s(L_o/4) + 1/s\,C_{Co-GND})} \quad (1)$$

$$Z_{Co-GND} \cong \frac{1/s\,C_{Co-GND} \cdot (s(L_o/4) + 1/s\,C_{MP-GND})}{1/s\,C_{Co-GND} + (s(L_o/4) + 1/s\,C_{MP-GND})} \quad (2)$$

The solution for this system of equations is not analytical and must be found numerically. Using the measurement data from Fig. 6 leads to $C_{Co-GND} \cong 283\,pF$ and $C_{MP-GND} \cong 141\,pF$.

All the parameters of the equivalent circuit of Fig. 4 are known. The remaining unknown variable is the CM noise source voltage spectrum for the voltage source u_{CM}. In order to obtain the spectrum for the voltage source u_{CM}, a simplified time domain simulation of the system is performed for the circuit of Fig. 1. The objective of the simulation is to measure voltages $u_{o+,PE}$ and $u_{o-,PE}$, so that the CM voltage can be computed with

$$u_{CM} = \frac{u_{o+,PE} + u_{o-,PE}}{2} \quad (3)$$

The simulated time behaviour of the CM voltage is depicted in Fig. 7. This voltage is formed by portions of
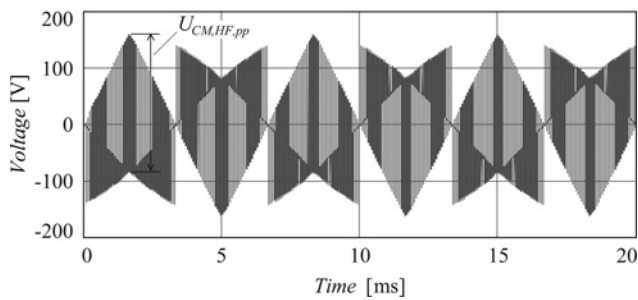
**Figure 7** *Time behaviour of the CM voltage u_{CM} computed with (3)*

the line-to-line voltages and has a maximum high-frequency peak-to-peak amplitude of approximately $U_{CM,HF,pp} = (3/\sqrt{8})U_{N,rms}$. With this, the CM voltage of the three-phase buck PWM rectifier is relatively small when compared to the CM voltage in boost-type rectifiers. The counterpart of that is that the DM emissions are larger because of the discontinuous input currents.

Computing the fast Fourier transform for the CM voltage leads to the spectrum presented in Fig. 8. The peak RMS voltage is approximately 45 V at the switching frequency (28 kHz) and the spectrum decays by -20 dB/decade up to $1/(\pi t_r) \cong 1.6$ MHz, from where -40 dB/decade follows.

In order to use the characteristics of this spectrum in a simplified way and use the experimental data regarding switching times, an envelope function is employed, defined with

$$s_{U_{CM}}(f) = \left| \frac{2\delta E}{(1 + \pi f \, \delta T_s)(1 + \pi f t_r)} \right| \qquad (4)$$

where, $E = U_{CM,HF,pp}/2$, $T_s = 1/28$ kHz is the switching period, $t_r = 200$ ns is the rise time estimated from switching loss measurements and $\delta = 0.23$ is the duty
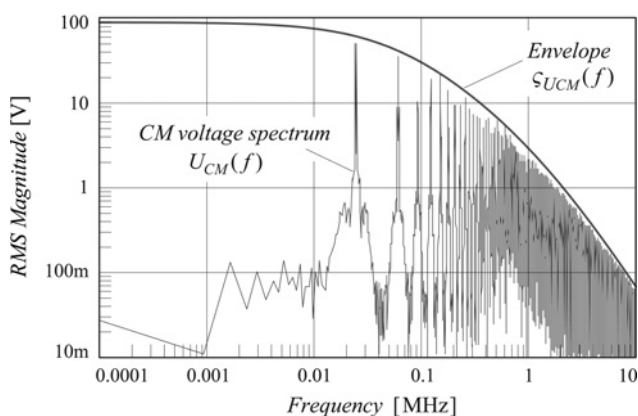
Figure 8 *Spectrum of the common mode voltage obtained through the simplified circuit simulation*

Also shown is the asymptotic curve for the employed envelope function $s_{U_{CM}}(f)$

ratio, which is found from the comparison with the computed spectrum, which is also displayed in Fig. 8.

2.2 Model verification

To verify the proposed CM propagation model, CE measurements employing an HF current probe Pearson 410 are performed. The probe presents a nominal bandwidth of 20 MHz, measuring the sum of the input currents as in Fig. 9. The gain of the current probe is adequately compensated in the performed CE measurements.

The measured conducted emission levels are compared to the estimated CE levels in Fig. 10. It is noticed that, the critical emission points are the peaks close to 250 and 600 kHz and, once these are lowered, the emissions at the lower boundary of the measurement band (150 kHz) become dominant. Thus, these are the frequencies that must be taken into account during the input CM filter design. Furthermore, the estimated conducted emissions envelope provides a highly correlated response when compared to the measured CE levels up to approximately 4 MHz, thus, validating the modelling procedure.
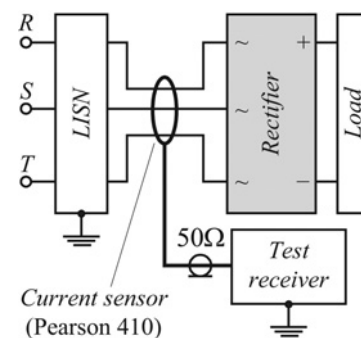
Figure 9 *CM measurement setup: the sum of the input currents is measured with a current probe Pearson 410 in order to obtain only the CM levels*
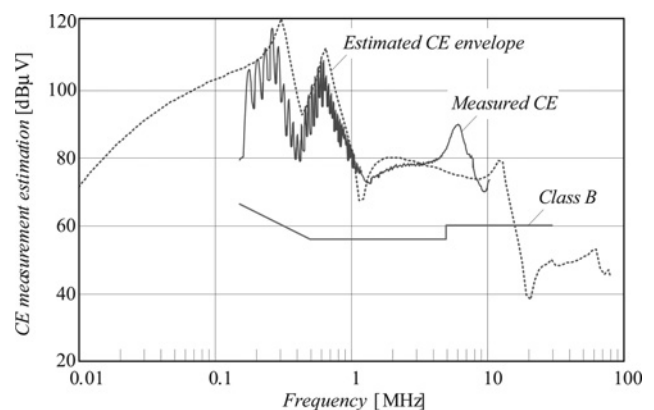
Figure 10 *CM emission levels at a three-lines LISN*

Shown are the measured levels and the predicted ones for a QP measurement as per CISPR 22

3 Common mode EMC input filter design

The main purpose of the CM input filter is to hinder the common mode current propagation to the mains by providing a high impedance in the direction to the mains and/or by providing paths with low impedance around the rectifier elements, which are responsible for the generation of CM voltages so that CM noise current is circulated back internally.
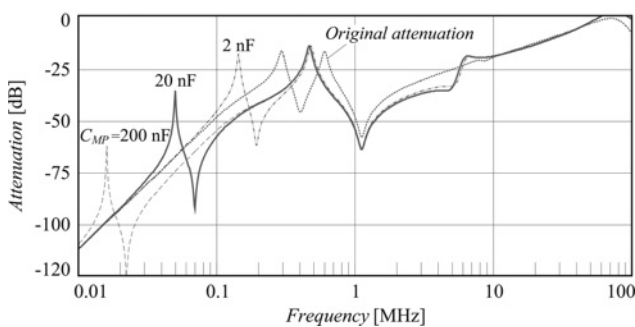
3.1 Effects of a capacitive connection from the input star-point to the output centre-point

In order to reduce CM emissions, a capacitance C_{MP} (cf. Fig. 11) is placed between the star-point of the DM input filter capacitors and the centre point of the output capacitors, allowing the HF common mode current to return, in some extent, to its source. The influence of this capacitive connection in the equivalent CM circuit of Fig. 11 is observed in Fig. 12, which also shows the original CM CE attenuation curve. It is seen that the strong resonance, originally at approximately 250 kHz can be shifted to lower frequencies. Thus, applying this connections leads to a lower filtering effort.
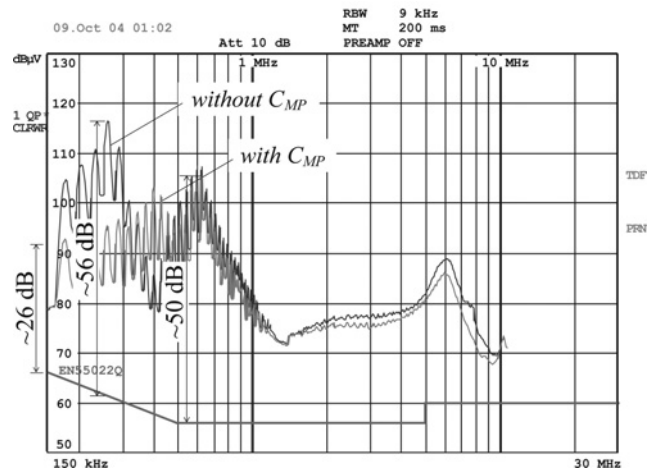
In the case at hand, $C_{MP} = 20$ nF was selected in order to shift the resonance at 250 kHz (cf. Fig. 13) to a frequency
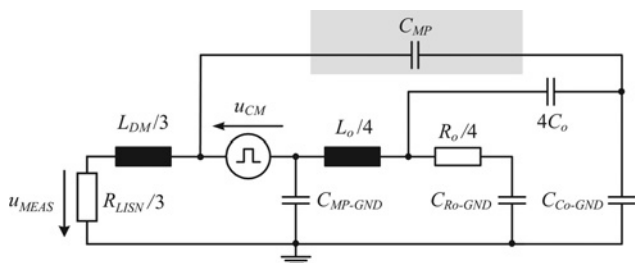
Figure 11 *Capacitive connection from output to input creates an alternative path for the CM currents, while not increasing earth leakage currents*

Figure 12 *Influence of different capacitance values of C_{MP} to the CM attenuation curves given by $U_{MEAS}(j\omega)/U_{CM}(j\omega)$*

Figure 13 *Effect of the capacitive connection (C_{MP}) from the star-point of the DM input filter capacitors to the rectifier output with $C_{MP} = 20$ nF*

The sum of the input currents is measured as in Fig. 9 to obtain only the CM signal. As the current measurement bandwidth is 20 MHz, the measurement is constrained to 10 MHz. Shown are the CE measurement without the inclusion of any CM filtering elements and after the inclusion of the capacitive connection with C_{MP}

below 150 kHz. In practice two capacitors $C_{MP}/2 = 10$ nF have been connected to the positive and negative output capacitor terminals. The effect of this connection is shown in Fig. 13 by CM-conducted emission measurements employing the same setup as in Fig. 9.

3.2 Two-stage CM filter design

For guaranteeing compliance to Class B limits, Fig. 13 shows that the attenuation with a CM filter must be higher than -50 dB around 600 kHz and higher than -26 dB at 150 kHz. Additional margin of 6 dB is considered as suggested in CISPR 11. In order to reduce the total size of the CM filter, the attenuation is distributed to two filter stages [23] as presented in the following.

The total capacitance $C_{CM,total} = C_{CM,1} + C_{CM,2}$ between any of the input phases and PE is restrained by the maximum allowable earth leakage $I_{GND,rms}$ current because of IT safety regulations. The tests are performed usually with 110% of the input RMS voltage $U_{N,rms}$ and the leakage current [24] should be typically limited to $I_{GND,rms} \leq 3.5$ mA, even for the case where one of the phases is lost.

With the leakage current given by

$$I_{GND,rms} = 1.1 \cdot U_{N,rms} \cdot 2\pi \cdot 50 \, \text{Hz} \cdot C_{CM,total} \qquad (5)$$

a maximum total CM capacitance per phase of $C_{CM,total} \cong 44$ nF is reached. Providing a margin and guaranteeing small footprints for the capacitors, the values of $C_{CM,1} = C_{CM,2} = 4.7$ nF are selected resulting in a total CM capacitance of 9.4 nF per phase. With two of the filter

elements selected, the next step is the determination of the inductors.

As the designed filter is built with two LC stages (cf. Fig. 15), a high slope in the attenuation is achieved. Owing to this new circuit configuration, the resonance peak at 600 kHz is changed. Thus, if the filter components are selected to fulfil the attenuation requirement at 150 kHz (-32 dB), the slope provided by the multistage filter attenuation provides a high attenuation at 600 kHz. For this reason, the CM filter is designed for the requirement at 150 kHz.

As the CM voltage is relatively small, the CM inductor can be built with small cores. Applying a smaller $L_{CM,1}$ and larger $L_{CM,2}$ leads to a large CM impedance at the mains side. This has the advantage of reducing the influence of the mains in the filtering performance. The total required attenuation $Att_{CM,req}$ at 150 kHz is divided into two parts, $Att_{CM,1} \cong -10$ dB and $Att_{CM,2} \cong -22$ dB. With these values, the required impedances for the inductors $L_{CM,1}$ and $L_{CM,2}$ are computed for the two critical cases as

$$Z_{LCM,1,req} \cong 210\,\Omega@150\,kHz \qquad (6)$$

$$Z_{LCM,2,req} \cong 820\,\Omega@150\,kHz \qquad (7)$$

With this, the filter inductors are built as specified in Table 1, which also presents the specifications for the capacitors in the CM filter. Passive damping through resistors is not added because of the predominantly resistive high frequency behaviour of the inductors (cf. Fig. 14) built with core material VITROPERM 500F [25]. These inductors exhibit good impedance stability for high temperatures and high power density.

The effect of the addition of the filtering components to the single-phase equivalent circuit of the final filter structure as shown in Fig. 15 can be observed in Fig. 16 through the plots of the transfer function $U_{MEAS}(j\omega)/U_{CM}(j\omega)$ for the different circuit configurations. The final filter configuration is able to provide the required attenuation in the complete frequency range and the peak at 600 kHz no longer exists. Employing the attenuation curves of Fig. 16 and applying $s_{U_{CM}}(f)$, the final CE levels are estimated in Fig. 17.

Table 1 CM filter components

| Component	Specification
$C_{CM,1}$, $C_{CM,2}$	Y1 Capacitor, Epcos MKP B81123
	4.7 nF−250 Vac
C_{MP}	Y1 Capacitor, Epcos MKP B81123
	2×10 nF−250 Vac
$L_{CM,1}$	Vaccuumschmelze VAC VITROPERM 500F W409
	$N = 3 \times 4$ turns, AWG 16
$L_{CM,2}$	Vaccuumschmelze VAC VITROPERM 500F W380
	$N = 3 \times 7$ turns, AWG 16
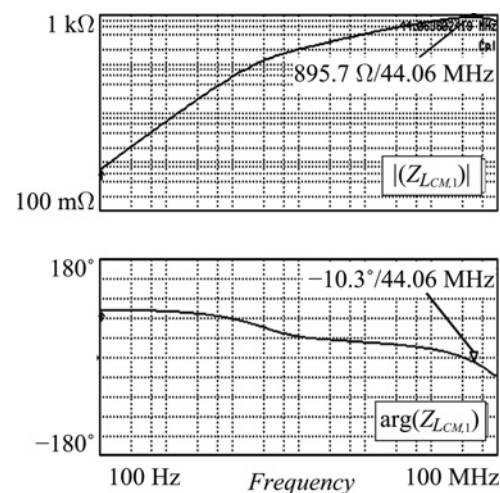
Figure 14 *Impedance measurement for the inductor $L_{CM,1}$*

A well-damped high-frequency behaviour and a high self resonance frequency (≈ 44 MHz) can be observed. The impedance at 150 kHz is measured as 240 Ω

3.3 Experimental verification

The final circuit schematic for the rectifier system including the CM filtering components is shown in Fig. 15. As the DM filter design has been previously proven in [5],
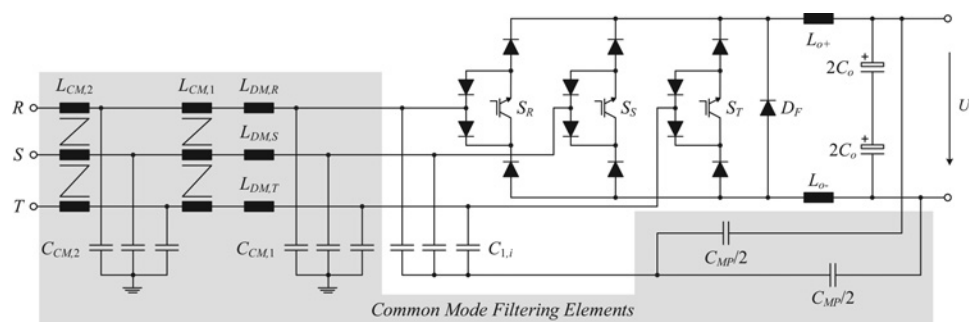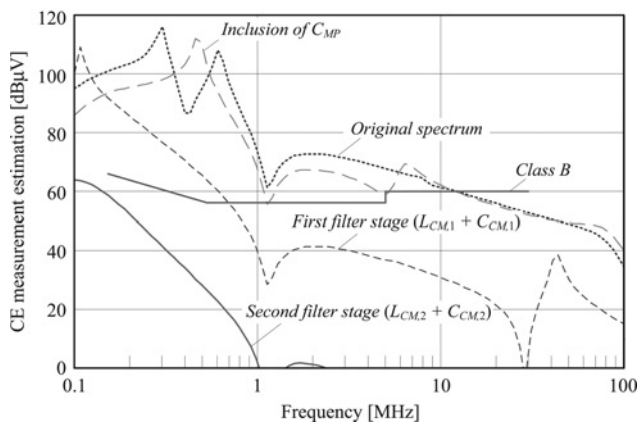

Figure 15 *Final circuit structure for the three-phase PWM rectifier system including the designed CM input filter*

215
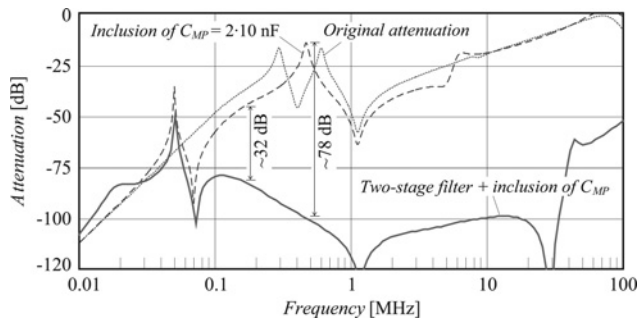
Figure 16 *Attenuation plots*

Shown are the different attenuation curves of the transfer function $U_{MEAS}(j\omega)/U_{CM}(j\omega)$ for different filter configurations, clarifying the effects of the insertion of each filtering components to the CM attenuation

Figure 17 *Estimated CM conducted emission levels for different circuit configurations and employing the CM voltage envelope $s_{U_{CM}}(f)$*
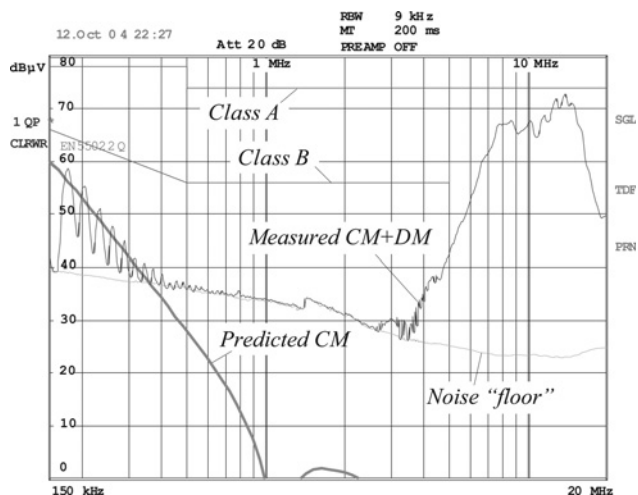
Figure 18 *Conducted emissions measurement according to CISPR 22 of the rectifier ($U_{N,l-l,rms} = 400$ V, $U_o = 400$ V, $P_o = 5$ kW) including the proposed CM filter and the DM filter*

This measurements were performed at the output terminals from a LISN (not with a current transducer)

the final experiments have been performed by measuring the total noise as required in CISPR 16. Fig. 18 shows the final result of the CE measurement performed with a four-lines 50 Ω/50 μH LISN according to CISPR 16 [26]. The measurement is done in order to test the compliance of the rectifier and includes both CM and DM emissions from the 5 kW hardware prototype. Obviously, the CM noise emissions are sufficiently attenuated, and Class A is fulfilled in the frequency range 150 kHz–20 MHz. For fulfilling Class B the emission levels that increase around 10 MHz would have to be properly attenuated. This can be achieved through shielding of the EMC input filter and of the rectifier unit. Owing to the superposition of the CM and DM emissions the predicted curve lies slightly below the observed peaks. Furthermore, the measurement noise-floor prevents from observing the behaviour beyond 400 kHz. Nevertheless, the dimensioning of the CM filter is validated.

4   Conclusions

A model for the CM propagation in a three-phase buck-type PWM rectifier has been presented. This model is based in very simple simulations, from where CM and DM noise sources are derived. The propagation paths are modelled with the employment of equivalent impedance circuits, which are obtained from direct measurements performed in the individual components and in the power converter in order to define parasitic impedances. This model has been compared with conducted emission measurements performed with a 5 kW prototype, from where it is observed a very good correlation up to a frequency of 4 MHz.

The design of a CM filter for a three-phase PWM rectifier is performed based on a CM noise propagation model, which is parameterised by simple impedance measurements on an existing converter prototype. The proposed model, along with a previous CE EMC measurement, allows a sufficiently accurate prediction of the required CM filter attenuation and a straight-forward design. With this, no complex modelling of the noise paths is required.

A capacitive connection between the star-point of the DM input filter capacitors and the output capacitor has been analysed and additionally contributes to the attenuation of the CM noise through the modification of the noise propagation. The relevant points for a successful CM filter design have been discussed. For the case at hand, the reduction of the CM emissions from 150 to 600 kHz has been identified as the most relevant range. The selection of the filtering components is presented and their main characteristics are explained.

Finally, measurements on a hardware prototype verify the theoretical considerations and the successful CM filter design.

5   References

[1]   GONG G., HELDWEIN M.L., DROFENIK U., MINIBOCK J., MINO K., KOLAR J.W.: 'Comparative evaluation of three-phase high-power-factor ac−dc converter concepts for application in future more electric aircraft', *IEEE Trans. Ind. Electron.*, 2005, **52**, (3), pp. 727−737, (0278-0046)

[2]   MALESANI L., TENTI P.: 'Three-phase ac/dc pwm converter with sinusoidal ac currents and minimum filter requirements', *IEEE Trans. Ind. Appl.*, 1987, **23**, (1), pp. 71−77

[3]   PIRES V.F., SILVA J.F.: 'Three-phase single-stage four-switch pfc buck-boost-type rectifier', *IEEE Trans. Ind. Electron.*, 2005, **52**, (2), pp. 444−453, (0278-0046)

[4]   NUSSBAUMER T., HELDWEIN M.L., GONG G., ROUND S.D., KOLAR J.W.: 'Comparison of prediction techniques to compensate time delays caused by digital control of a three-phase buck-type pwm rectifier system', *IEEE Trans. Ind. Electron.*, 2008, **55**, (2), pp. 791−799, (0278-0046)

[5]   NUSSBAUMER T., HELDWEIN M.L., KOLAR J.W.: 'Difierential mode input filter design for a three-phase buck-type pwm rectifier based on modeling of the emc test receiver', *IEEE Trans. Ind. Electron.*, 2006, **53**, (5), pp. 1649−1661, (0278-0046)

[6]   BAUMANN M., KOLAR J.W.: 'Parallel connection of two three-phase three-switch buck-type unity-power-factor rectifier systems with dc-link current balancing', *IEEE Trans. Ind. Electron.*, 2007, **54**, (6), pp. 3042−3053, (0278-0046)

[7]   BAUMANN M., KOLAR J.W.: 'A novel control concept for reliable operation of a three-phase three-switch buck-type unity power factor rectifier with integrated boost output stage under heavily unbalanced mains condition', *IEEE Trans. Ind. Electron.*, 2005, **52**, (2), pp. 399−409

[8]   NUSSBAUMER T., GONG G., HELDWEIN M.L., KOLAR J.W.: 'Modeling and robust control of a three-phase buck + boost pwm rectifier (vrx-4)', *IEEE Trans. Ind. Appl.*, 2008, **44**, (2), pp. 650−662, (0093-9994)

[9]   NAVE M.J.: 'Power line filter design for switched-mode power supplies' (Van Nostrand Reinhold, New York, USA, 1991)

[10]   WILLIAMS T.: 'EMC for product engineers' (Elsevier Ltd, Oxford, UK, 2007, 4th edn.)

[11]   HELDWEIN M.L., NUSSBAUMER T., BECK F., KOLAR J.W.: 'Novel three-phase cm/dm conducted emissions separator'. IEEE Applied Power Electronics Conf. on Exposition, 2005, vol. 2, pp. 797−802

[12]   MENG J., MA W., PAN Q., ZHAO Z., ZHANG L.: 'Noise source lumped circuit modeling and identification for power converters', *IEEE Trans. Ind. Electron.*, 2006, **53**, (6), pp. 1853−1861, (0278-0046)

[13]   JIN M., WEIMING M.: 'Power converter emi analysis including igbt nonlinear switching transient model', *IEEE Trans. Ind. Electron.*, 2006, **53**, (5), pp. 1577− 1583, (0278-0046)

[14]   YANG L., ODENDAAL W.G.H.: 'Measurement-based method to characterize parasitic parameters of the integrated power electronics modules', *IEEE Trans. Power Electron.*, 2007, **22**, (1), pp. 54−62, (0885-8993)

[15]   CHEN J.Z., YANG L., BOROYEVICH D., ODENDAAL W.G.: 'Modeling and measurements of parasitic parameters for integrated power electronics modules'. IEEE Applied Power Electronics Conf. on Exposition, 2004, vol. 1, pp. 522−525

[16]   GITAU M.N.: 'Modeling conducted emi noise generation and propagation in boost converters'. IEEE Int. Symp. on Industrial Electronics, 2000, vol. 2, pp. 353−358

[17]   POON N.K., PONG B.M.H., LIU C.P., TSE C.K.: 'Essential coupling path models for non-contact emi in switching power converters using lumped circuit elements', *IEEE Trans. Power Electron.*, 2003, **18**, (2), pp. 686−695, (0885-8993)

[18]   DROFENIK U.: 'Optimierung und experimentelle Analyse des stationaeren Betriebsverhaltens eines VIENNA Rectifier I'. PhD thesis, Technischen Universitaet Wien, 1998

[19]   TOOTH D.J., FINNEY S.J., WILLIAMS B.: 'Fourier theory of jumps applied to converter harmonic analysis', *IEEE Trans. Aerosp. Electron. Syst.*, 2001, **37**, (1), pp. 109−122, (0018-9251)

[20]   LIU Q., SHEN W., WANG F., BOROYEVICH D., STEFANOVIC V., ARPILLIERE M.: 'Experimental evaluation of igbts for characterizing and modeling conducted emi emission in pwm inverters'. Power Electronics Special. Conf., 2003, vol. 4, pp. 1951−1956

[21]   RAN L., GOKANI S., CLARE J., BRADLEY K.J., CHRISTOPOULOS C.: 'Conducted electromagnetic emissions in induction motor drive systems. i. Time domain analysis and identification of dominant modes', *IEEE Trans. Power Electron.*, 1998, **13**, (4), pp. 757−767, (0885-8993)

[22]   FLOREAN D., SPIAZZI G.: 'Common mode filter project by means of internal impedance measurements'. IEEE Int. Symp. on Electromagnetic Compatibility, 2000, vol. 2, pp. 541−545

[23] NAGEL A.: 'Leitungsgebundene Stoerungen in der Leistungselektronik: Entstehung, Ausbreitung und Filterung'. PhD thesis, Rheinisch-Westfaelischen Hochschule Aachen, 2001

[24] IEC: 'Safety of information technology equipment – IEC 60950'. International Electrotechnical Commission – IEC, Brussels, Belgium, 1999

[25] Vacuumschmelze: 'Nanocrystalline Vitroperm EMC components' (Vacuumschmelze (VAC) GmbH and Co, Hanau, 2004)

[26] CISPR: 'C.I.S.P.R. Specification for radio interference measuring apparatus and measurement methods – publication 16'. IEC Int. Special Committee on Radio Interference – C.I.S.P.R, 1977